Journal of
Computational and Theoretical Nanoscience
Vol. 7, 1–17, 2010

Electric-Field Induced Transitions in a Cholesteric Liquid-Crystal Film with Negative Dielectric Anisotropy

E. C. Gartland Jr.[1,*], H. Huang[1], O. D. Lavrentovich[2], P. Palffy-Muhoray[2], I. I. Smalyukh[3], T. Kosa[4], and B. Taheri[4]

[1] *Department of Mathematical Sciences, Kent State University, Kent, Ohio 44242, USA*
[2] *Liquid Crystal Institute, Kent State University, Kent, Ohio 44242, USA*
[3] *Department of Physics, University of Colorado at Boulder, Boulder, Colorado 80309, USA*
[4] *AlphaMicron, Inc., 277 Martinel Drive, Kent, Ohio 44240, USA*

A combination of analytical, numerical, and qualitative methods is used to study competing equilibrium orientational configurations in a liquid-crystal thin film. The material is a cholesteric liquid crystal and has a negative dielectric anisotropy. The system has strong homeotropic anchoring of the liquid-crystal director on the confining substrates and is subject to a voltage applied across the film thickness. A free-energy functional embodies the competing influences of the boundary conditions, the intrinsic chirality of the material, and the electric field. Attention is restricted to director fields that are functions only of the distance across the cell gap. A detailed phase and bifurcation analysis of the two equilibrium configurations of this type is presented; the control parameters are the ratio of the cell gap to the intrinsic pitch of the cholesteric and the applied voltage. The study was motivated by potential technological applications. The phase diagram contains both first-order and second-order transition lines, the former terminating at an isolated point and the latter at a triple point. The voltage-dependent nature of the total twist of the director across the cell is revealed and explained, and an effective upper bound is obtained on the ratio of cell gap to pitch for the system to support a simple voltage-driven second-order transition between the two 1-D equilibrium states.

Keywords: Liquid Crystals, Thin Films, Cholesterics, Oseen-Frank Free Energy, Negative Dielectric Anisotropy, Phase and Bifurcation Analysis.

RESEARCH ARTICLE

1. INTRODUCTION AND MODEL

Cholesteric liquid crystals (also known as chiral nematics), in the absence of any other influences, form a twisting equilibrium orientational ground state with the liquid crystal "director" (the local average orientation of the long axes of the molecules) rotating transverse to a helical axis, the direction of which is degenerate in space. Because of their unique optical properties, these materials are used in several liquid-crystal-based technologies, including displays, switchable diffraction gratings, eyewear with voltage-controlled transparency, beam-steering devices, and mirror-less lasers, among others.[1–12] The understanding of the orientational structures in cholesteric-liquid-crystal systems, and the transitions among them, is of practical importance, as well as of fundamental interest. It is the subject of this paper, in which we study a particular cholesteric-liquid-crystal system (geometry, boundary conditions, material properties) that is used in some of these applications.[a]

We report on an analysis of the structural phase and bifurcation behavior of equilibrium molecular orientational configurations in a thin cholesteric-liquid-crystal film. The material also has a "negative dielectric anisotropy;" this causes the director to prefer to align perpendicular to an electric field, which for the system we study is parallel to the film normal. In addition, the substrates that confine the film are treated in such a way as to encourage the director to align perpendicular adjacent to the substrate (i.e., parallel to the applied electric field)—so called "homeotropic" alignment. The competition among these several influences (intrinsic chirality, electric field, and boundary conditions)

*Author to whom correspondence should be addressed.

[a] Standard references on the physics of liquid crystals are Priestly et al.,[13] Vertogen and de Jeu,[14] Pikin,[15] Chandrasekhar,[16] de Gennes and Prost,[17] and Kleman and Lavrentovich.[18] For the mathematics of liquid crystals, we refer to Ericksen and Kinderlehrer,[19] Virga,[20] and Stewart.[21]

leads to multiple equilibrium orientational states and complex transitions among them.

This system (basic geometry, orientations, and material properties) underlies technologies discussed in Refs. [1, 3, 6, 10]. The motivation for our work was as part of a combined experimental and analytical study of this system with a particular (proprietary) material being evaluated for potential commercial applications in such areas. This basic system (with various different materials) has been much studied from experimental, qualitative, and numerical points of view.[22–27] The most interesting equilibrium configurations are functions of two space dimensions, one being across the cell gap, periodic in one direction in the plane of the film. A variety of such textures and transitions appear in the references above. An overview can be found in Ref. [27], which also contains a reproduction of previously reported phase diagrams (extended to include the influence of different boundary alignment treatments and the presence or absence of spacers), as well as the unambiguous reconstruction of the complex periodic director fields using fluorescence confocal polarizing microscopy (which validated some previously suggested models and disproved others).

The present paper is concerned with the competition between two one-dimensional equilibrium states, which are functions only of the distance across the cell gap (uniform in the plane of the film)—we will report on the more complicated periodic instabilities at a future time. These two configurations (referred to below as "Homeotropic" and "Translation Independent Cholesteric") and the transition between them are used in electrically driven light shutters, intensity modulators, eyewear with tunable transparency, and displays, as discussed in Refs. [1, 3, 6, 10]. Our analysis will reveal a phase diagram that is more complicated than one would expect and which has implications for technologies based on these configurations and transitions. The geometry of the system and the coordinate system we shall use are displayed in Figure 1. Of the several different

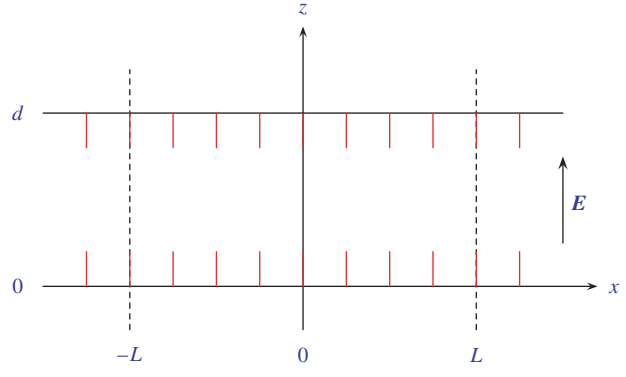

Fig. 1. Thin film geometry and coordinate system: cell gap d, period of periodic-in-x solutions $2L$ (not known a-priori), electric field $\boldsymbol{E}$. Perfect homeotropic anchoring (perpendicular alignment) of the liquid-crystal director is assumed at the boundaries adjacent to the upper and lower substrates. All fields are uniform in y.

equilibrium configurations observed experimentally, we concentrate on the three depicted in Figure 2, where we employ the terminology of Ref. [26].

The "Homeotropic" configuration is stable for sufficiently small cell gaps and voltages, when the boundary conditions can overcome both the intrinsic chirality (and desire of the director to form a pure-twist ground state) as well as the influence of the electric field (which encourages the director to align perpendicular to the field, in the horizontal direction). This configuration has a completely uniform director field. For sufficiently large cell gap and/or sufficiently high voltage, the "Translation Independent Cholesteric" (TIC) configuration can exist. It is sometimes locally stable (metastable) and sometimes, in addition, globally stable (minimum free energy). It is nonuniform in the z direction only (across the cell gap) and is rotationally degenerate: any continuous rotation of it around the z axis produces an equivalent equilibrium director field (with the same free energy). 1-D-periodic structures can also exist for sufficiently large cell gaps and voltages, and these compete with the Homeotropic and TIC solutions. The "Cholesteric Finger of type 1" (CF1) is one of the most common—see Figure 2 right, where a single period is displayed. This configuration is periodic in the lateral, x, direction and translationally degenerate: any continuous translation in the x direction produces an equivalent equilibrium director field. All solutions we consider are uniform in the y direction.

We model the system with Oseen-Frank elasticity and coupled electrostatic potential: the free energy (per unit length in the y direction) of a single period in the x direction is given by

$$\mathcal{F}[\boldsymbol{n}, \psi] = \int_{-L}^{L}\int_{0}^{d} \sigma(\boldsymbol{n}, \nabla\boldsymbol{n}, \nabla\psi)\, dz\, dx \tag{1}$$

where $\boldsymbol{n} = \boldsymbol{n}(x, z)$ is the director (a unit-length vector field), $\psi = \psi(x, z)$ the electrostatic potential ($\boldsymbol{E} = -\nabla\psi$, the local electric field), and the free-energy density is given by

$$\begin{aligned} 2\sigma = {} & K_1(\operatorname{div}\boldsymbol{n})^2 + K_2(\boldsymbol{n}\cdot\operatorname{curl}\boldsymbol{n} + q_0)^2 + K_3|\boldsymbol{n}\times\operatorname{curl}\boldsymbol{n}|^2 \\ & - \varepsilon_0[\varepsilon_\perp|\nabla\psi|^2 + \varepsilon_a(\nabla\psi\cdot\boldsymbol{n})^2] \end{aligned} \tag{2}$$

Here L is the half-period of a periodic-in-x solution; d is the cell gap; $q_0 = 2\pi/P$ is the wavenumber associated with the intrinsic "pitch" P of the cholesteric; and ε_0 is the vacuum dielectric permittivity (8.854×10^{-12} F/m). The values of the Frank elastic constants K_1, K_2, and K_3 for the particular material used in our experiments are given in Table I, as are the relative dielectric constants $\varepsilon_\parallel$ (relative dielectric permittivity parallel to the electric field) and $\varepsilon_\perp$ (relative permittivity perpendicular to the field). The "dielectric anisotropy" is their difference, which is *negative* for our material: $\varepsilon_a := \varepsilon_\parallel - \varepsilon_\perp$. The material is proprietary; the material parameters were measured

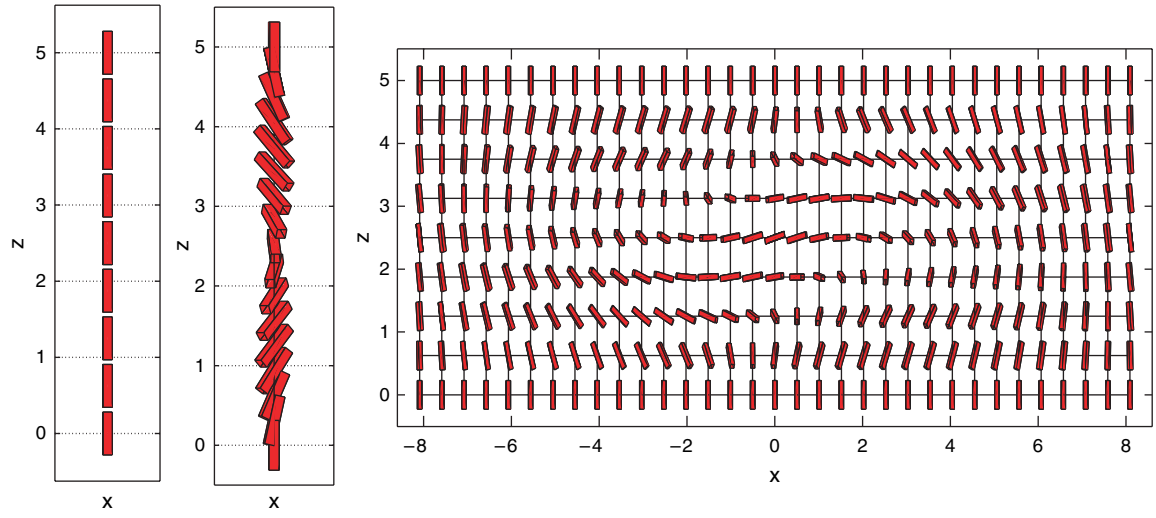

Fig. 2. Equilibrium director fields: "Homeotropic" (left), "Translation Independent Cholesteric" (TIC, center), "Cholesteric Finger of type 1" (CF1, right, one period). Lengths are in microns.

experimentally (using Fréedericksz thresholds to determine the elastic constants and using capacitance measurements for the dielectric constants)—details can be found in Ref. [27].

The first three terms of (2) embody the "elastic energy" associated with distortions of the director field. Were q_0 equal to *zero* (the case of a nematic liquid crystal), the zero-distortional-energy ground state would be a uniform field $\boldsymbol{n} = \text{const}$ (for which both $\operatorname{div}\boldsymbol{n} = 0$ and $\operatorname{curl}\boldsymbol{n} = \boldsymbol{0}$). For $q_0 \neq 0$, the zero-elastic-energy state is given by fields of the general form

$$\boldsymbol{n}(z) = \cos q_0 z \boldsymbol{e}_x + \sin q_0 z \boldsymbol{e}_y \tag{3}$$

where the helical axis ($\boldsymbol{e}_z$ above) could be oriented in any arbitrary direction; for such fields we have $\operatorname{div}\boldsymbol{n} = 0$ and $\operatorname{curl}\boldsymbol{n} = -q_0\boldsymbol{n}$ ($\Rightarrow \boldsymbol{n}\cdot\operatorname{curl}\boldsymbol{n} + q_0 = 0$ and $\boldsymbol{n}\times\operatorname{curl}\boldsymbol{n} = \boldsymbol{0}$). The last two terms of (2) embody the free energy associated with the electric-field/liquid-crystal interaction. With a given electric field (given $\nabla\psi$), the free-energy density σ is minimized by $\boldsymbol{n} \perp \nabla\psi$ ($\boldsymbol{n}\cdot\nabla\psi = 0$) for $\varepsilon_a < 0$ (our case), as opposed to $\boldsymbol{n} \parallel \nabla\psi$ for $\varepsilon_a > 0$.

The periodicity $2L$ is not known or specified a-priori. In this general setting, the constrained, coupled equilibrium equations satisfied by the director field $\boldsymbol{n} = \boldsymbol{n}(x, z)$ and electrostatic potential $\psi = \psi(x, z)$ can be expressed

$$-\operatorname{div}\left(\frac{\partial\sigma}{\partial\nabla\boldsymbol{n}}\right) + \frac{\partial\sigma}{\partial\boldsymbol{n}} = \lambda\boldsymbol{n},$$

$$|\boldsymbol{n}| = 1,\ -\infty < x < \infty,\ 0 < z < d \tag{4a}$$

$$\operatorname{div}(\boldsymbol{\epsilon}(\boldsymbol{n})\nabla\psi) = 0, \quad \boldsymbol{\epsilon} = \varepsilon_0(\varepsilon_\perp\mathbf{I} + \varepsilon_a\boldsymbol{n}\otimes\boldsymbol{n}) \tag{4b}$$

Here $\lambda = \lambda(x, z)$ is the Lagrange-multiplier field associated with the pointwise unit-vector constraint on $\boldsymbol{n}$, and $\boldsymbol{\epsilon}$ is the dielectric tensor of a uniaxial crystal with optic axis $\boldsymbol{n}$. We follow some of the notation of Refs. [20] and [21]. In terms of Cartesian tensors, the following identifications can be made:

$$\left[\frac{\partial\sigma}{\partial\nabla\boldsymbol{n}}\right] = \frac{\partial\sigma}{\partial n_{\alpha,\beta}}, \quad \left[\frac{\partial\sigma}{\partial\boldsymbol{n}}\right] = \frac{\partial\sigma}{\partial n_\alpha}, \quad [\mathbf{I}] = \delta_{\alpha\beta}$$
$$[\boldsymbol{n}\otimes\boldsymbol{n}] = n_\alpha n_\beta, \quad \alpha,\beta = x, y, z \tag{5}$$

The boundary conditions are

$$\boldsymbol{n}(x, 0) = \boldsymbol{n}(x, d) = \boldsymbol{e}_z$$
$$\psi(x, 0) = 0, \quad \psi(x, d) = V \tag{6}$$

where V is the applied voltage. The globally stable "phase" of the system is given by the coupled equilibrium fields of least free energy—this is the configuration that would be observed in a laboratory experiment in general.

Two aspects of the modeling warrant discussion: the appropriateness of Frank elasticity and the assumption of infinitely strong homeotropic anchoring. The Oseen-Frank phenomenological theory is based on certain assumptions and has its limitations. It assumes a uniform degree of orientational order with a uniaxial molecular orientational distribution. It does not explicitly take into account molecular conformational variations. It also assumes mild spatial variations in the director field. It is a macroscopic

Table I. Material parameters: elastic constants (K_1, K_2, K_3, in units of $\text{pN} = 10^{-12}$ J/m) and relative dielectric permittivities ($\varepsilon_\parallel$, $\varepsilon_\perp$, dimensionless) associated with free-energy density (2).

K_1	17.2 pN
K_2	7.51 pN
K_3	17.9 pN
$\varepsilon_\parallel$	3.4
$\varepsilon_\perp$	7.1

RESEARCH ARTICLE

model, meant to be valid on length scales that are large compared to intrinsic, molecular-order length scales. This theory has been very successful in modeling systems of low-molecular-weight liquid crystals in super-micron-size geometries. Its validity is strained, for example, when dealing with cores of the singular defects,[18, 28] behavior close to the transition into the isotropic phase, high shear rates (in the related Ericksen-Leslie hydrodynamic theory), and the like.

The proprietary material used in the experiments we model is a low-molecular-weight liquid crystal with a typical nematic correlation length in the range of 10 s of nanometers. The cells (in both the experiments and in the technologies) are typically 5–10 microns thick (2–3 orders of magnitude larger than the correlation lengths) and free of defects, for the configurations we analyze. The applied AC voltages were sufficiently low and frequencies sufficiently high to avoid hydrodynamic instabilities. See Ref. [27] for details on the experiments. All these circumstances suggest that the Oseen-Frank model should perform quite well.

Perpendicular ("normal" or "homeotropic") orientation of the nematic director at the interface of a liquid crystal and various media is a well established experimental fact, whose mechanisms are discussed, for example, by Sonin in Refs. [29] and Yokoyama in Ref. [30]. A variety of techniques can be used to achieve the homeotropic orientation; it is often established at the free surface of nematic liquid crystals formed by polar molecules or at the interfaces containing amphiphilic (surfactant) molecules. In particular, in Ref. [27] (Smalyukh et al., the experiments we model), the homeotropic alignment has been established at the interface between a low-molecular-weight cholesteric mixture and a commercially available polyimide coating JALS-204 (JSR, Japan). When such a polyimide is unidirectionally rubbed and when the director is forced to tilt away from the normal orientation (for example, by an external electric field), this unidirectional treatment helps to reduce the manifold of distorted configurations.[27]

An important issue is the relative strength of the molecular interactions that keep the director in the homeotropic position. The relevant measure of this is the so-called (polar) anchoring coefficient W (see, e.g., Refs. [18, 29, 30]), which is determined by the work needed to deviate the director by a certain angle from the normal to the interface, per unit area of the interface. The ratio $l = K/W$, where K is the typical Frank elastic constant, has the dimension of length and is called the anchoring "extrapolation length."[18] If l is much smaller than the typical spatial scale of director distortions, then the search for an equilibrium configuration is reduced to the minimization of the Frank-Oseen functional with no additional surface terms. This is the case in our work: in the relevant experimental situation described in Ref. [27], l has been estimated to be in the sub-micrometer range, while the other length scales, such as the cell thickness, the cholesteric pitch, the length scale of director reorientation, are much larger, in the range of 2–100 micrometers.

Thus the boundary conditions in our case are taken into account by simply requiring that the director at the surface does not deviate from the normal orientation. This approach is often called "infinitely strong anchoring" or "fixed boundary conditions" (see, e.g., Refs. [17, 18]). The "weak anchoring" (finite-strength anchoring) regime could have been built into the model, at the expense of an added surface anchoring term to the Frank-Oseen functional and thus some additional complexity but not much deeper insight; such an addition was not deemed necessary for the first stage of modeling of the structures with the director varying over scales much larger than the submicron distance l.

2. DIRECTOR ANGLE REPRESENTATION AND REDUCED SYSTEMS

To gain some preliminary understanding of this system, we have restricted our consideration in this paper to configurations that are *uniform* in x, i.e., "1-D" solutions, which are functions of z only. This excludes the CF1 configuration. In this first phase of our investigation, then, we study the bifurcation and phase behavior of the Homeotropic versus TIC solutions, under the assumption that all fields are functions of z only.

2.1. Director Angle Representation and Equilibrium Equations

For the analysis of these 1-D solutions, a representation of the director field in terms of spherical-polar coordinates is useful:

$$n_x = \sin\theta\cos\varphi, \quad n_y = \sin\theta\sin\varphi, \quad n_z = \cos\theta \tag{7}$$

In terms of these, the pointwise unit-vector constraint $|\boldsymbol{n}(z)| = 1$ is automatically satisfied, and the Homeotropic solution takes the form

$$\theta(z) = 0 = \text{const}, \quad \varphi(z) = \text{undefined}, \quad \psi(z) = \frac{Vz}{d} \tag{8}$$

The components of the TIC solution cannot be expressed analytically (as far as we know). They can be computed numerically and, for representative parameter values, appear as in Figure 3. In terms of this angle representation of the director, the free-energy density becomes

$$\begin{aligned} 2\sigma = {} & (K_1\sin^2\theta + K_3\cos^2\theta)\theta_z^2 \\ & + (K_2\sin^2\theta + K_3\cos^2\theta)\sin^2\theta\varphi_z^2 \\ & - 2K_2 q_0 \sin^2\theta\varphi_z + K_2 q_0^2 \\ & - \varepsilon_0(\varepsilon_\perp\sin^2\theta + \varepsilon_\parallel\cos^2\theta)\psi_z^2 \end{aligned} \tag{9}$$

where $\theta_z = d\theta/dz$, etc.

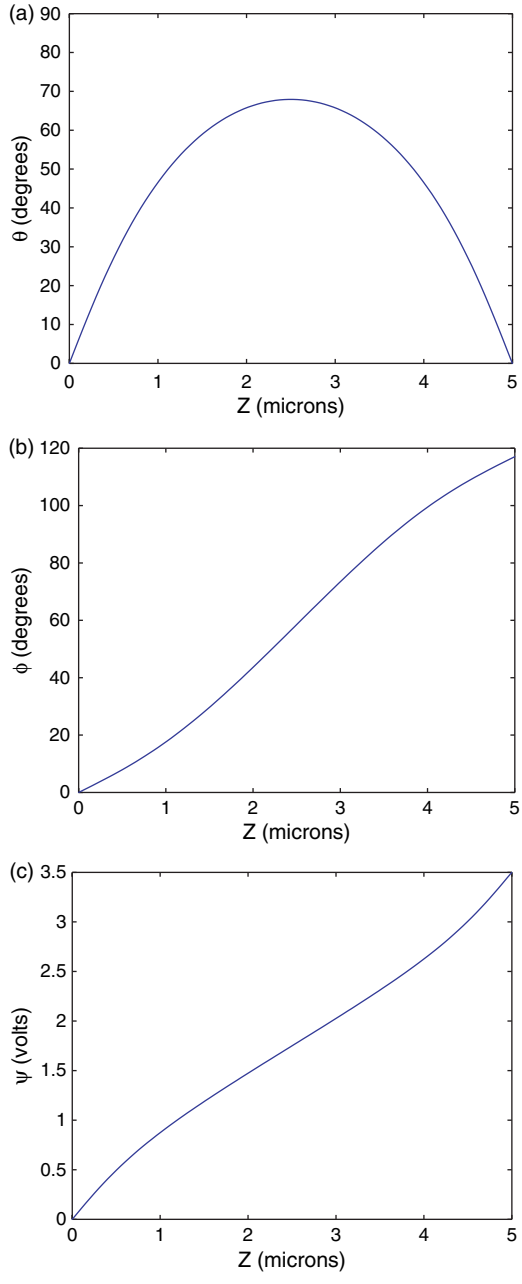

Fig. 3. Components of a representative TIC equilibrium solution (numerically computed): tilt angle (θ, top), twist angle (φ, center), and electrostatic potential (ψ, bottom) versus z (distance across the cell). Parameters: as in Table I, cell gap $d = 5\,\mu$m, d/P ratio $= 0.5$, voltage $V = 3.5$ volts.

The coupled Euler-Lagrange differential equations associated with (9) are given by

$$\frac{d}{dz}[(K_1 \sin^2\theta + K_3 \cos^2\theta)\theta_z] = \sin\theta\cos\theta\{(K_1 - K_3)\theta_z^2 + [(2K_2 - K_3)\sin^2\theta + K_3\cos^2\theta]\varphi_z^2 - 2K_2 q_0 \varphi_z + \varepsilon_0\varepsilon_a\psi_z^2\} \tag{10a}$$

$$\frac{d}{dz}\{\sin^2\theta[(K_2\sin^2\theta + K_3\cos^2\theta)\varphi_z - K_2 q_0]\} = 0 \tag{10b}$$

$$\frac{d}{dz}[(\varepsilon_\perp \sin^2\theta + \varepsilon_\parallel \cos^2\theta)\psi_z] = 0 \tag{10c}$$

with associated boundary conditions

$$\theta(0) = \theta(d) = 0, \quad \varphi(0),\ \varphi(d) \text{ undefined}, \quad \psi(0) = 0, \quad \psi(d) = V \tag{11}$$

These give necessary conditions for equilibria. This problem as it stands is degenerate because of the rotational invariance of the TIC solutions and associated indeterminacy of the φ boundary conditions.

2.2. First Integrals and Reduced Systems

Equations (10b) and (10c) have right-hand sides of zero by virtue of the fact that the free-energy density (9) involves only the derivatives φ_z and ψ_z and not the undifferentiated fields φ and ψ. As a result, these equations can be integrated directly to give the first integrals

$$(K_2\sin^2\theta + K_3\cos^2\theta)\varphi_z = K_2 q_0 + \frac{c_1}{\sin^2\theta} \tag{12}$$

and

$$(\varepsilon_\perp \sin^2\theta + \varepsilon_\parallel \cos^2\theta)\psi_z = \frac{V}{\int_0^d 1/(\varepsilon_\perp \sin^2\theta + \varepsilon_\parallel \cos^2\theta)\,dz} \tag{13}$$

the latter having used as well the boundary conditions on ψ. From (13) we can obtain an explicit formula for the electrostatic potential in terms of the equilibrium θ field for the director:

$$\psi(z) = V\frac{\int_0^z 1/(\varepsilon_\perp \sin^2\theta(\zeta) + \varepsilon_\parallel \cos^2\theta(\zeta))\,d\zeta}{\int_0^d 1/(\varepsilon_\perp \sin^2\theta(\zeta) + \varepsilon_\parallel \cos^2\theta(\zeta))\,d\zeta} \tag{14}$$

The fate of the integration constant c_1 in (12) can be determined by examining its role in the free-energy density σ. If we use the expression (12) above to replace the terms in (9) involving φ_z by their equilibrium equivalents involving θ only, we find that

$$(K_2\sin^2\theta + K_3\cos^2\theta)\sin^2\theta\varphi_z^2 - 2K_2 q_0 \sin^2\theta\varphi_z = -K_2 q_0^2 \frac{K_2\sin^2\theta}{K_2\sin^2\theta + K_3\cos^2\theta} + \frac{c_1^2}{\sin^2\theta(K_2\sin^2\theta + K_3\cos^2\theta)} \tag{15}$$

The term containing c_1^2 above is nonnegative and so would give a free-energy-minimizing state only when $c_1 = 0$. Moreover, by virtue of the boundary conditions on $\theta(z)$ ($\theta(0) = \theta(d) = 0$), we see that near the boundary points

RESEARCH ARTICLE

$z = 0$ and $z = d$, the $\sin^2\theta$ factor in the denominator of this term should behave like

$$\sin^2\theta(z) = \theta_z(0)^2 z^2 + O(z^4), \quad \text{near } z = 0 \tag{16}$$

and

$$\sin^2\theta(z) = \theta_z(d)^2 (d-z)^2 + O((d-z)^4), \quad \text{near } z = d \tag{17}$$

which would cause the integral of this term to be divergent. Thus (granted that θ_z remains bounded) the only choice of c_1 that leads to admissible equilibrium fields is $c_1 = 0$. Thus we obtain

$$\begin{aligned} (K_2 \sin^2\theta + K_3 \cos^2\theta)\varphi_z &= K_2 q_0 \\ \Delta\varphi &= \int_0^d \frac{K_2 q_0}{K_2 \sin^2\theta + K_3 \cos^2\theta}\, dz \end{aligned} \tag{18}$$

Here $\Delta\varphi$ denotes the "total twist" across the cell.

The expressions (13) and (18) enable us to remove φ and/or ψ from the system. The free-energy density with φ removed takes the form

$$\begin{aligned} 2\sigma = {} & (K_1 \sin^2\theta + K_3 \cos^2\theta)\theta_z^2 \\ & + K_2 q_0^2 \frac{K_3 \cos^2\theta}{K_2 \sin^2\theta + K_3 \cos^2\theta} \\ & - \varepsilon_0(\varepsilon_\perp \sin^2\theta + \varepsilon_\parallel \cos^2\theta)\psi_z^2 \end{aligned} \tag{19}$$

while the free energy with both φ and ψ removed is given by

$$\begin{aligned} \mathcal{F}[\theta] = {} & \frac{1}{2}\int_0^d \left[(K_1 \sin^2\theta + K_3 \cos^2\theta)\theta_z^2 \right. \\ & \left. + K_2 q_0^2 \frac{K_3 \cos^2\theta}{K_2 \sin^2\theta + K_3 \cos^2\theta} \right] dz \\ & - \frac{1}{2}\varepsilon_0 V^2 \left[\int_0^d \frac{1}{\varepsilon_\perp \sin^2\theta + \varepsilon_\parallel \cos^2\theta}\, dz \right]^{-1} \end{aligned} \tag{20}$$

This latter expression is similar to Ref. [21, Eq. (3.221), p. 91], where the approach of Deuling[31] to analyze a Fréedericksz transition with an electric field is discussed; the formula above for our free energy includes an additional term from the intrinsic chirality, which is not present in the case in Refs. [21, 31].

Equation (18) expresses the dependence of the local (instantaneous) "twist rate," $\varphi_z(z)$, on the tilt angle. Since the elastic constants for our material satisfy $K_2 \approx K_3/2$, the twist rate varies between roughly $q_0/2$, for $\theta \approx 0$, to the usual bulk value of q_0, for $\theta \approx \pi/2$. The total twist across a cell of thickness d then satisfies

$$\pi \frac{d}{P} \approx 2\pi \frac{K_2}{K_3}\frac{d}{P} < \Delta\varphi < 2\pi \frac{d}{P} \tag{21}$$

approaching the lower limit for very small voltages and the upper limit for very large voltages.

3. PERTURBATION ANALYSIS OF BIFURCATIONS

We study the local linear stability of the Homeotropic solution with respect to 1-D (z-dependent only) perturbations. We do this first by expanding the free energy (20) around the $\theta(z) = 0$ equilibrium state and analyzing the quadratic form associated with the second variation, finding that the uniform state is stable within a certain ellipse in the $(d/P, V)$ parameter plane. Preliminary numerical explorations reveal that the transition from Homeotropic to TIC can be either "first order" (discontinuous with respect to changes in the dependent variables) or "second order" (continuous), and so we then perform a more refined perturbation analysis of the Homeotropic-TIC bifurcation points (for different material parameters) to try to determine where in the parameter space the change from one behavior to the other takes place.

3.1. Local Stability of Homeotropic Configuration

The local stability of the Homeotropic configuration to perturbations, which we are restricting to be uniform in x (as well as y), can be analyzed in various ways. If we introduce a small perturbation of the uniform ground state $\theta(z) = 0 + \delta\theta(z)$, $|\delta\theta| \ll 1$, into the θ-only form of the free energy in (20) and expand, we obtain

$$\begin{aligned} \mathcal{F}[0+\delta\theta] = {} & \frac{1}{2}\left[K_2 q_0^2 d - \frac{\varepsilon_0 \varepsilon_\parallel V^2}{d} \right] \\ & + \frac{1}{2}\int_0^d \left[K_3 \delta\theta_z^2 + \left(\frac{\varepsilon_0 \varepsilon_a V^2}{d^2} - \frac{K_2^2 q_0^2}{K_3} \right)\delta\theta^2 \right] \\ & + O(\delta\theta^4) \end{aligned} \tag{22}$$

Here the leading term gives the free energy of the Homeotropic $\boldsymbol{n}(z) = \boldsymbol{e}_z$ director field, and the first-order terms vanish by virtue of the equilibrium conditions satisfied by it. The second term in the expansion is a quadratic form in the perturbation $\delta\theta(z)$; it is positive definite for V^2 and q_0^2 sufficiently small—keep in mind that $\varepsilon_a < 0$. By examining the eigenvalue problem associated with this form, one can deduce that stability is lost to a perturbing mode of the form $\delta\theta(z) \propto \sin \pi z/d$ when the pair $(d/P, V)$ is outside the "spinodal ellipse"

$$\frac{4K_2^2}{K_3^2}\left(\frac{d}{P}\right)^2 - \frac{\varepsilon_0 \varepsilon_a}{K_3 \pi^2} V^2 = 1 \tag{23}$$

This equation is consistent with Refs. [24, 26]. The loss of stability can be either 1st order, for d/P large, or 2nd order, for d/P small. The situation is depicted in Figure 4.

3.2. Nondimensionalization

The point on the spinodal ellipse at which the bifurcation changes from supercritical to subcritical can be determined

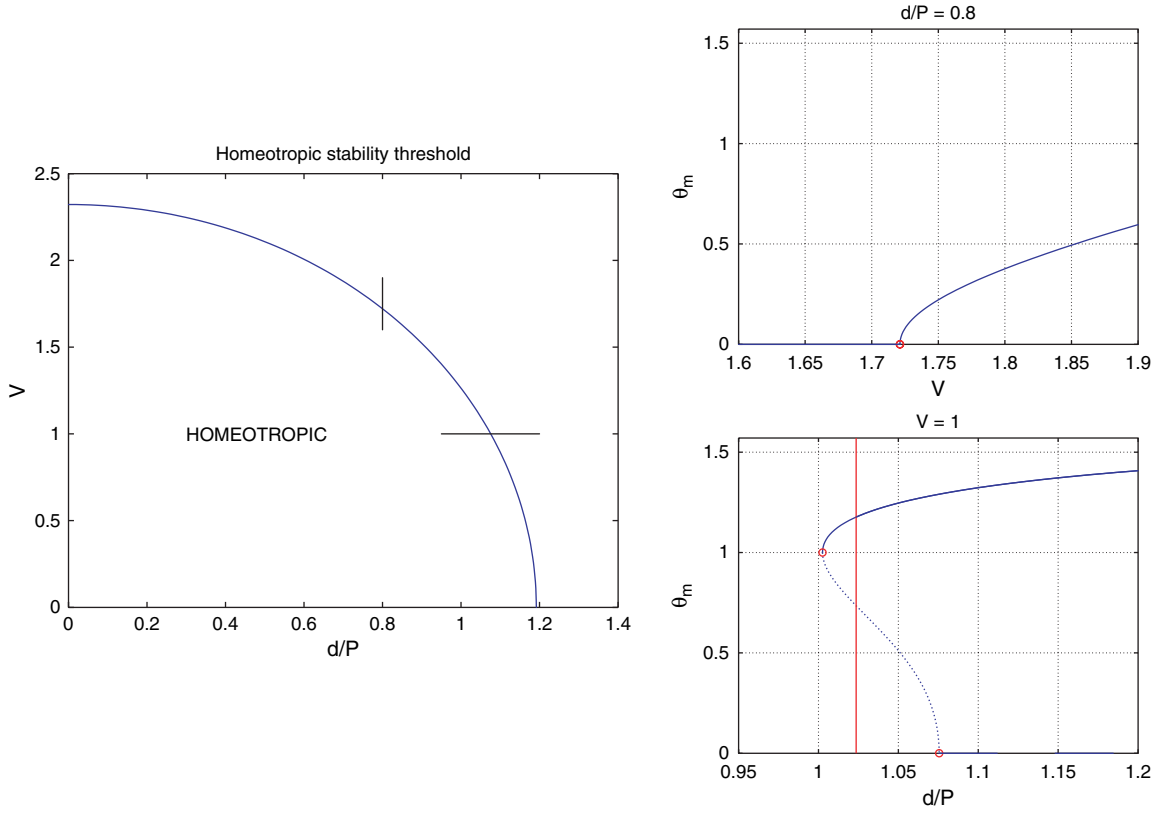

Fig. 4. Metastability limit (spinodal ellipse) for Homeotropic equilibrium director field (left). The black lines at $d/P = 0.8$ and $V = 1.0$ volts indicate scan lines for the bifurcation diagrams on the right. The bifurcation diagrams plot the maximum tilt angle θ_m versus voltage V for constant $d/P = 0.8$ (upper right) and θ_m versus d/P for constant $V = 1.0$ volts (lower right). Only the upper parts of the mirror-symmetric pictures are shown. The upper-right bifurcation diagram is "supercritical" (associated with a 2nd-order transition); while the lower-right is "subcritical" (1st-order transition). In the bifurcation diagrams, metastable configurations are indicated with solid blue lines; dashed blue lines correspond to equilibria that are not locally stable. The global free-energy-minimizing solution is indicated with a heavier blue line; the vertical red line corresponds to the crossover point. The value $\theta_m = 0$ corresponds to the Homeotropic solution; values of $\theta_m \neq 0$ are associated with TIC solutions.

in various ways. Here we do so by performing a perturbation analysis of the bifurcation points that occur at all the points along this curve. For this we find it convenient to use the θ-only formulation of the equilibrium equations. The Euler-Lagrange equation associated with (20) is given by

$$\frac{d}{dz}[(K_1\sin^2\theta + K_3\cos^2\theta)\theta_z]$$
$$= \sin\theta\cos\theta\left\{(K_1-K_3)\theta_z^2 - K_2 q_0^2\frac{K_2K_3}{(K_2\sin^2\theta+K_3\cos^2\theta)^2}\right.$$
$$+\frac{\varepsilon_0\varepsilon_a V^2}{(\varepsilon_\perp\sin^2\theta+\varepsilon_\parallel\cos^2\theta)^2}$$
$$\left.\times\left[\int_0^d\frac{1}{\varepsilon_\perp\sin^2\theta+\varepsilon_\parallel\cos^2\theta}\,dz\right]^{-2}\right\} \quad (24)$$

to be solved on $0 < z < d$ subject to boundary conditions $\theta(0) = \theta(d) = 0$. The problem is nonlinear, and it is nonlocal—due to the fact that the local electric field (associated with the ψ_z term in (9), which has been removed) depends on the orientation of the director across the entire cell. Observe that the problem possesses mirror symmetry: if $\theta(z)$ satisfies (24), then so must $-\theta(z)$. This is the cause of the "pitchfork" nature of the bifurcations.

It is advantageous at this stage to put our problem in dimensionless form. To this end we introduce

$$\bar{z} := \frac{\pi z}{d}, \quad \bar{\theta}(\bar{z}) := \theta(z), \quad \bar{\varepsilon}_a := \frac{\varepsilon_a}{\varepsilon_\parallel} = \frac{\varepsilon_\parallel - \varepsilon_\perp}{\varepsilon_\parallel} \quad (25a)$$

and

$$k_1 := \frac{K_1-K_3}{K_3}, \quad k_2 := \frac{K_2-K_3}{K_3},$$
$$\alpha := \sqrt{\frac{-\varepsilon_0\varepsilon_a}{K_3}}\frac{V}{\pi}, \quad \beta := \frac{K_2 q_0 d}{K_3\pi} \quad (25b)$$

in terms of which (24) takes the form (after dropping bars)

$$\frac{d}{dz}[(1+k_1\sin^2\theta)\theta_z]$$
$$= \sin\theta\cos\theta\left\{k_1\theta_z^2 - \frac{\beta^2}{(1+k_2\sin^2\theta)^2} - \frac{\alpha^2}{(1-\bar{\varepsilon}_a\sin^2\theta)^2}\right.$$
$$\left.\times\left[\frac{1}{\pi}\int_0^\pi\frac{1}{1-\bar{\varepsilon}_a\sin^2\theta}\,dz\right]^{-2}\right\} \quad (26)$$

which is to be solved on $0 < z < \pi$ subject to boundary conditions $\theta(0) = \theta(\pi) = 0$. Here we regard k_1, k_2, and $\bar{\varepsilon}_a$ as "material" parameters and α and β as "control" or "continuation" parameters. The dimensionless parameter α is proportional to the voltage V, while β is proportional to the d/P ratio—recall that $q_0 = 2\pi/P$. Numerical values for k_1, k_2, and $\bar{\varepsilon}_a$ for the material used in our experiments (see Table I) are given by

$$k_1 \doteq -0.039, \quad k_2 \doteq -0.580, \quad \bar{\varepsilon}_a \doteq -1.088 \tag{27}$$

We also note that in terms of α and β, the spinodal ellipse (23) becomes the unit circle in the $\alpha - \beta$ parameter plane

$$\alpha^2 + \beta^2 = 1 \tag{28}$$

3.3. Perturbation Analysis of Bifurcation Points

We restrict our attention to scenarios of the types depicted in Figure 4: β fixed, continuation with respect to α, or α fixed, with continuation in β. Other (α, β) trajectories are possible. Considering the former of these, we introduce a continuation parameter η and formally expand around a possible bifurcation point at $\eta = 0$:

$$\theta(z;\eta) = \theta_1(z)\eta + \theta_3(z)\eta^3 + \theta_5(z)\eta^5 + \cdots \tag{29a}$$

$$\alpha(\eta) = \alpha_0 + \alpha_2\eta^2 + \alpha_4\eta^4 + \cdots \tag{29b}$$

The oddness of the θ expansion (with respect to η) and evenness of the α expansion are consistent with the symmetry of the problem; if one seeks θ and α in terms of more general expansions, one finds the terms omitted above to be zero.

We require a normalization for the parameter η, and we adopt the following (for convenience):

$$\frac{4}{\pi}\int_0^\pi \left(\frac{\partial\theta}{\partial\eta}\right)^2 dz + 3\left(\frac{d\alpha}{d\eta}\right)^2 = 2 \tag{30}$$

This gives η the significance of a pseudo-arc-length parameter in $\theta - \alpha$ space. The consequences of this normalization at the first few orders are

$$O(1): \quad \frac{2}{\pi}\int_0^\pi \theta_1^2\, dz = 1 \tag{31a}$$

$$O(\eta^2): \quad \frac{2}{\pi}\int_0^\pi \theta_1\theta_3\, dz + \alpha_2^2 = 0 \tag{31b}$$

$$O(\eta^4): \quad \frac{9}{\pi}\int_0^\pi \theta_3^2\, dz + \frac{10}{\pi}\int_0^\pi \theta_1\theta_5\, dz + 12\alpha_2\alpha_4 = 0 \tag{31c}$$

Formally substituting the assumed expansions (29) into (26), we obtain at leading order, $O(\eta)$,

$$\theta_1'' + (\alpha_0^2 + \beta^2)\theta_1 = 0$$
$$0 < z < \pi,\ \theta_1(0) = \theta_1(\pi) = 0 \tag{32}$$

which will have nontrivial solutions only if

$$\alpha_0^2 + \beta^2 = m^2, \quad m = 1, 2, \ldots \tag{33}$$

The first unstable mode corresponds to $m = 1$, and we obtain

$$\alpha_0^2 + \beta^2 = 1, \quad \theta_1(z) = A_{1,1}\sin z \tag{34}$$

The normalization condition (31a) implies that $A_{1,1}^2 = 1$, and we choose the positive values

$$\alpha_0 = \sqrt{1-\beta^2}, \quad A_{1,1} = 1 \tag{35}$$

At the next order, $O(\eta^3)$, we obtain the problem for θ_3, which has the form

$$\theta_3'' + \theta_3 = C_{3,1}\sin z + C_{3,3}\sin 3z$$
$$0 < z < \pi,\ \theta_3(0) = \theta_3(\pi) = 0 \tag{36}$$

with $C_{3,1}$ and $C_{3,3}$ given by

$$2C_{3,1} = k_1 + 1 - \bar{\varepsilon}_a + (3k_2 + \bar{\varepsilon}_a)\beta^2 - 4\alpha_0\alpha_2 \tag{37}$$

and

$$-6C_{3,3} = 3k_1 + 1 - 3\bar{\varepsilon}_a + 3(k_2 + \bar{\varepsilon}_a)\beta^2 \tag{38}$$

The solvability condition for (36) requires that the right-hand side of the ordinary differential equation be L^2-orthogonal to $\sin z$ (i.e., $\int_0^\pi f(z)\sin z\, dz = 0$, where f denotes the right-hand-side function), which implies that $C_{3,1} = 0$. This determines α_2,

$$4\alpha_0\alpha_2 = k_1 + 1 - \bar{\varepsilon}_a + (3k_2 + \bar{\varepsilon}_a)\beta^2, \quad \alpha_0 = \sqrt{1-\beta^2} \tag{39}$$

and the solution θ_3 of (36) then takes the form

$$\theta_3(z) = A_{3,1}\sin z + A_{3,3}\sin 3z, \quad A_{3,3} = -\frac{1}{8}C_{3,3} \tag{40}$$

The normalization condition (31b) yields

$$A_{3,1} = -\alpha_2^2 \tag{41}$$

If desired, this process could be continued. The problems at the next orders have a similar, clean overall structure; however the formulas for the coefficients become progressively more complicated. At $O(\eta^5)$ we would have

$$\theta_5'' + \theta_5 = C_{5,1}\sin z + C_{5,3}\sin 3z + C_{5,5}\sin 5z$$
$$0 < z < \pi,\ \theta_5(0) = \theta_5(\pi) = 0 \tag{42}$$

The formulas for $C_{5,1}$, $C_{5,3}$, and $C_{5,5}$ are quite long. Solvability again implies that $C_{5,1} = 0$, which determines α_4; the solution θ_5 takes the form

$$\theta_5(z) = A_{5,1}\sin z + A_{5,3}\sin 3z + A_{5,5}\sin 5z$$
$$A_{5,3} = -\frac{1}{8}C_{5,3},\ A_{5,5} = -\frac{1}{24}C_{5,5} \tag{43}$$

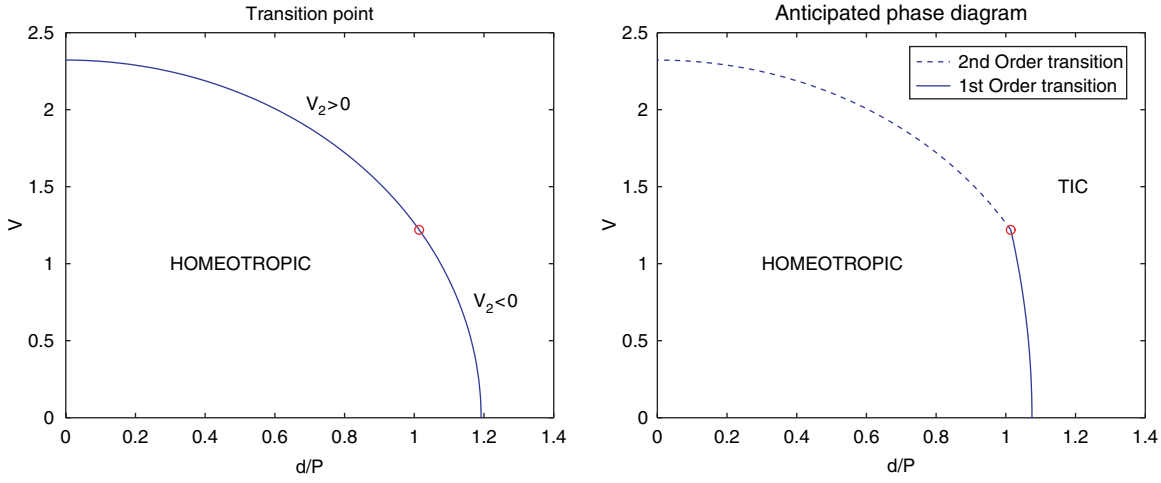

Fig. 5. Metastability region of Homeotropic configuration with transition point indicated (left). The bifurcation from Homeotropic to TIC is supercritical where the parameter $V_2 = \pi\sqrt{-K_3/\varepsilon_0\varepsilon_a}\alpha_2$ is positive; it is subcritical where V_2 is negative. The red circle denotes the transition point at which V_2 changes sign; its coordinates are $(d/P)_* \doteq 1.014$, $V_* = 1.220$ volts for our material parameters. On the right is a conjecture of what we might expect the phase diagram to look like, indicating a 2nd-order phase transition where the bifurcation is supercritical, with a 1st-order transition line anticipated to lie somewhere beyond that, in the region where the two solutions coexist, with location determined by the locus of free-energy crossover points.

and the normalization condition (31c) determines $A_{5,1}$. And so on. Beyond a certain point, a direct numerical approach (as we shall discuss in the next section) becomes more expedient.

At the moment, the most useful piece of information we have obtained is the expression (39) for α_2 in terms of the parameters k_1, k_2, $\bar{\varepsilon}_a$, and β. The sign of α_2 determines the forward or backward nature of the symmetry breaking pitchfork bifurcation: $\alpha_2 > 0$ implies a forward-opening ("supercritical") bifurcating branch, while $\alpha_2 < 0$ corresponds to a backward-opening ("subcritical") branch. For our material, the sub-expressions on the right-hand side of (39) have the following signs

$$k_1 + 1 - \bar{\varepsilon}_a > 0 \quad \text{and} \quad 3k_2 + \bar{\varepsilon}_a < 0 \tag{44}$$

with the change of sign occurring at the transition point

$$\begin{aligned} \alpha_* &= \sqrt{1-\beta_*^2} \doteq 0.525 \\ \beta_* &= \sqrt{\frac{-k_1 - 1 + \bar{\varepsilon}_a}{3k_2 + \bar{\varepsilon}_a}} \doteq 0.851 \end{aligned} \tag{45}$$

For the experimental work (see Refs. [24, 26, 27]), information has typically been expressed in terms of the applied voltage V and the ratio d/P. These are related to α and β by

$$V = \pi\sqrt{\frac{-K_3}{\varepsilon_0\varepsilon_a}}\alpha, \quad \frac{d}{P} = \frac{K_3}{2K_2}\beta \tag{46}$$

which for our material parameters gives rise to the crossover point

$$V_* \doteq 1.220 \text{ volts}, \quad \left(\frac{d}{P}\right)_* \doteq 1.014 \tag{47}$$

This point is indicated as the red circle in Figure 5 along with a conjecture of the kind of phase diagram we might expect on the basis of this analysis. The actual phase diagram is more complicated, as we shall now see.

4. NUMERICAL INVESTIGATION OF PHASES AND BIFURCATIONS

The actual phase diagram, for this case in which we artificially impose the constraint that the fields be functions of z only, is not as simple as anticipated above. It requires numerical techniques to explore. For this we have used the `MATCONT` software package.[32] `MATCONT` is a public-domain `MATLAB`® [b] toolbox for numerical continuation and bifurcation analysis of ordinary differential equations and general nonlinear algebraic systems. We use it to explore the equilibrium solutions of the coupled $\theta - \psi$ system, with φ removed. We utilize the dimensional forms, with the parameters of the material used in our experiments.

4.1. Numerical Bifurcation and Phase Analysis

From (19), the free energy with φ removed is given by

$$\begin{aligned} \mathcal{F}[\theta,\psi] = \frac{1}{2}\int_0^d \Big[&(K_1\sin^2\theta + K_3\cos^2\theta)\theta_z^2 \\ &+ K_2 q_0^2 \frac{K_3\cos^2\theta}{K_2\sin^2\theta + K_3\cos^2\theta} \\ &- \varepsilon_0(\varepsilon_\perp\sin^2\theta + \varepsilon_\parallel\cos^2\theta)\psi_z^2 \Big] dz \end{aligned} \tag{48}$$

[b] `MATLAB` is a registered trademark of The MathWorks, Inc.

We wish to compute equilibria (subject to boundary conditions $\theta(0)=\theta(d)=0$, $\psi(0)=0$, and $\psi(d)=V$), assess their local stability, and determine which equilibrium configurations have the least free energy. To this end, we discretize the free-energy functional (48) directly by a piecewise-linear finite-element method on a uniform grid with nodal quadrature:

$$z_k=k\Delta z,\ k=0,\ldots,n,\quad \Delta z=\frac{d}{n},\ \ \theta_k\approx\theta(z_k),\ \ \psi_k\approx\psi(z_k) \tag{49}$$

This results in a discrete free-energy that is a function of the interior (θ,ψ) nodal degrees of freedom in the general form

$$f(\theta_1,\ldots,\theta_{n-1},\psi_1,\ldots,\psi_{n-1}) =\sum_{k=0}^{n-1}\sigma_h(\theta_k,\theta_{k+1},\psi_k,\psi_{k+1})\Delta z \tag{50}$$

with $\theta_0=\theta_n=0$, $\psi_0=0$, $\psi_n=V$, and σ_h given by

$$\begin{aligned}
&4\sigma_h(\theta_0,\theta_1,\psi_0,\psi_1)\\
&=[K_1(\sin^2\theta_0+\sin^2\theta_1)+K_3(\cos^2\theta_0+\cos^2\theta_1)]\left(\frac{\theta_1-\theta_0}{\Delta z}\right)^2\\
&\quad+K_2q_0^2\left[\frac{K_3\cos^2\theta_0}{K_2\sin^2\theta_0+K_3\cos^2\theta_0}+\frac{K_3\cos^2\theta_1}{K_2\sin^2\theta_1+K_3\cos^2\theta_1}\right]\\
&\quad-\varepsilon_0[\varepsilon_\perp(\sin^2\theta_0+\sin^2\theta_1)\\
&\qquad+\varepsilon_\parallel(\cos^2\theta_0+\cos^2\theta_1)]\left(\frac{\psi_1-\psi_0}{\Delta z}\right)^2
\end{aligned} \tag{51}$$

Discrete equilibria are given by solutions of the gradient equations,

$$\frac{\partial f}{\partial\theta_1}=\cdots=\frac{\partial f}{\partial\theta_{n-1}}=\frac{\partial f}{\partial\psi_1}=\cdots=\frac{\partial f}{\partial\psi_{n-1}}=0 \tag{52}$$

a sparsely coupled nonlinear system of $2n-2$ equations in $2n-2$ unknowns. The local stability is assessed by examining the eigenvalues of the Hessian matrix

$$H=\left[\frac{\partial^2 f}{\partial x_i\partial x_j}\right]_{i,j=1}^{2n-2},\quad \boldsymbol{x}=(\theta_1,\ldots,\theta_{n-1},\psi_1,\ldots,\psi_{n-1}) \tag{53}$$

On a stable branch, H will have $n-1$ positive eigenvalues and $n-1$ negative ones (corresponding to the always-negative-definite $\psi_1,\ldots,\psi_{n-1}$ components). On an unstable branch, there will be fewer than $n-1$ positive eigenvalues. The existence of a *zero* eigenvalue indicates a singular point of the system and a potential bifurcation or fold point, at which an exchange of stability could take place. The free energies of multiple, competing, locally stable solutions can be compared directly using (50).

We favor a numerical approach such as this because it produces a discrete free energy, equilibrium equations, and stability eigenvalue problems that are consistent with each other, one following directly from the other. The approach used here is a low-order (2nd-order accurate) discretization approach, with the errors in the free energy and field variables proportional to Δz^2 (in theory and in our benchmarking). A viable alternative would be to use a "spectral" method, Fourier or polynomial based, in which θ and $\psi-Vz/d$ could approximated by truncated sums of modes $\{\sin\pi z/d,\sin 2\pi z/d,\ldots\}$, for example. This would have the advantage of requiring far fewer degrees of freedom to achieve comparable accuracy; however the analytics would be a bit more complicated, and the numerical linear algebra would involve full, dense (rather than sparse) matrices. We did not implement this latter approach.

The accuracy of the material parameters we have (determined by experiment, in Table I) is believed to be roughly three significant digits, which is about the level of visual discernment in a graph or plot, and so we adopted that as the target numerical accuracy for our computations. Thus we continued to refine our grids until all bifurcation points, limit points, free-energy-crossover points, and solution branches were stable at that level; this was achieved with $n=128$.[c]

4.2. Homeotropic-TIC Phase Diagram

The actual phase diagram that results is given in Figure 6. Its structure is somewhat close to what was anticipated; however, the 1st-order Homeotropic-TIC transition line does not terminate in the transition point as expected. Instead it crosses the spinodal ellipse at a different point, extends beyond the ellipse, and terminates in an isolated critical point (a cusp point). The perturbation analysis is correct, and there is indeed a change from supercritical to subcritical bifurcation at the identified transition point (the lower of the two red circles); however, it is associated with the development of a second, metastable, smaller amplitude TIC solution, and a second limit point. The scenario is illuminated in Figure 7.

We see that the small-amplitude TIC solution germinates at the transition point (red circle in lower right-hand corner of blowup region, Fig. 6 right, Fig. 7 top), when the applied voltage exceeds $V_*\doteq 1.220$ volts. The small- and large-amplitude TIC solutions coexist in the region beyond the spinodal ellipse between the limit-point loci denoted by the red lines. They undergo a 1st-order transition across

[c]Various implementation issues arise in using a numerical bifurcation package such as this, which was originally designed for small-scale autonomous ODE dynamical systems. One needs to take advantage of `MATLAB`'s sparse-matrix representations and solvers, and for this, one must use `MATCONT`'s @pde_1 "curve file." The Jacobian (our Hessian (53)) needs to be exactly symmetric (not just symmetric to roundoff level). Also, the package does not have a built-in capability of switching branches at a symmetry-breaking bifurcation point—such a singular point has a higher co-dimension than a simple bifurcation point, which the package is equipped to handle—and so an ad-hoc approach must be implemented to deal with such points.

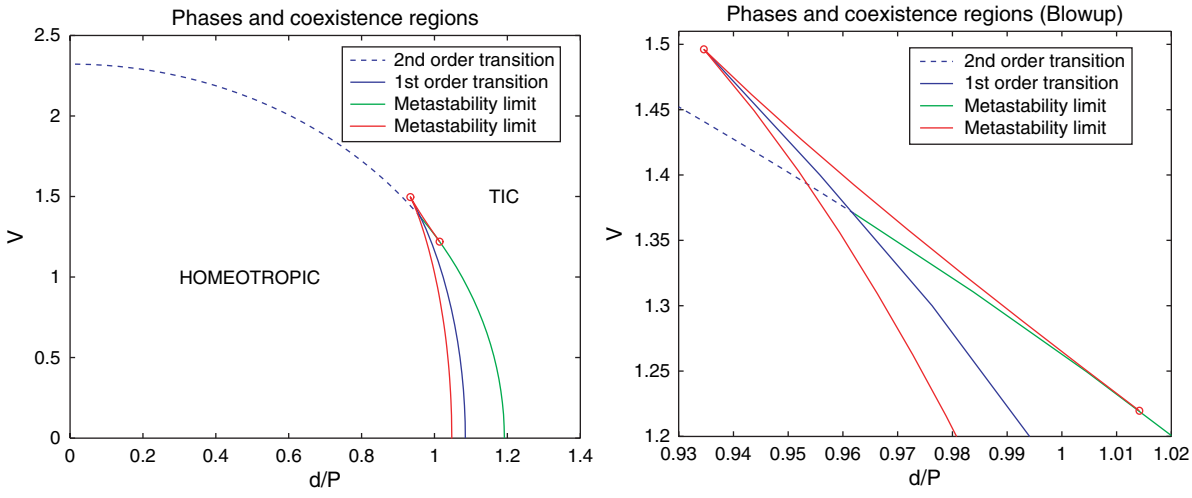

Fig. 6. Homeotropic-TIC phase diagram (left) and blowup (right). The dashed blue line indicates a 2nd-order transition from Homeotropic to TIC. The solid blue line is a 1st-order transition line. Inside the spinodal ellipse, it corresponds to a 1st-order transition from Homeotropic to TIC. Outside the spinodal ellipse, it indicates a 1st-order transition from a small-amplitude TIC (left of the line) to a large-amplitude TIC (right of the line). The 1st-order transition line terminates at the point where these two TIC solutions coalesce into one. The green line is the spinodal ellipse, indicating the metastability limit of the Homeotropic solution. The red lines are spinodal lines for the TIC solutions: large amplitude (left), small amplitude (right). These correspond to loci of fold points that indicate the metastability limits of these phases. These lines terminate in the cusp point $d/P \doteq 0.935$, $V \doteq 1.496$ volts. The "triple point," where the 2nd-order transition line terminates at the 1st-order line, has coordinates $d/P \doteq 0.962$, $V \doteq 1.370$ volts.

the solid blue line in between. The two TIC solutions merge together when the limit points coalesce at the cusp point (red circle in upper-left corner of blowup region), the coordinates of which are $d/P \doteq 0.935$, $V \doteq 1.496$ volts. The complicated nonlinear behavior that we already see in this simplified version of our model (with our admissible fields and variations restricted to be functions of z only) is consistent with the picture obtained in the experiments (see

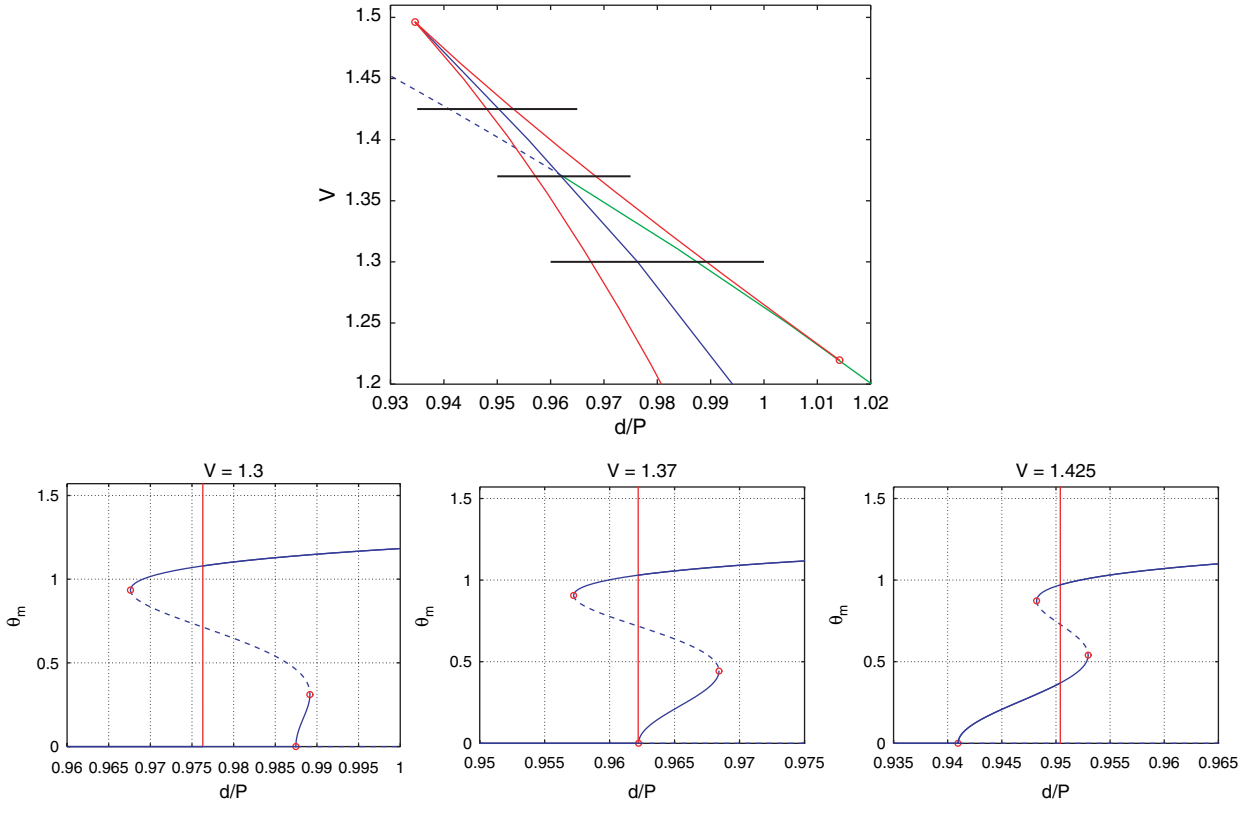

Fig. 7. Blowup of complicated part of Homeotropic-TIC phase diagram (upper). The horizontal black lines indicate scan lines, corresponding to values $V = 1.3$, 1.37, and 1.425 volts, of the bifurcation diagrams in the lower left, center, and right.

Ref. [27]) and in the analysis when we allow our fields to depend on both x and z (on which we will report later).

5. 2-D LOCAL STABILITY OF HOMEOTROPIC CONFIGURATION

The problematic solutions for this system are functions of *two* independent variables, x and z, such as the CF1 configuration. We would like to assess the stability of the Homeotropic solution to perturbations of this type, to see, for example, if there is ever a situation in which the Homeotropic solution loses local stability directly to a periodic-in-x solution, such as CF1. This is possible in principle and was the case, for example, for the system studied by Lonberg and Meyer[33] some time ago. The issue of which solution (Homeotropic, TIC, CF1) is *globally* stable (has lowest free energy) must be resolved numerically. Here we first just perform a local linear stability analysis of the Homeotropic configuration and show that it is *not* possible for it to lose local stability directly to a periodic-in-x solution when the control parameters are inside the spinodal ellipse.

5.1. General Linear Stability Criterion

The metastability of an equilibrium solution $(\boldsymbol{n}_0, \psi_0)$ can be assessed in various ways, here we adopt the point of view of the constrained director dynamical system

$$\gamma \frac{\partial \boldsymbol{n}}{\partial t} = P(\boldsymbol{n})\boldsymbol{h}(\boldsymbol{n}, \psi), \quad |\boldsymbol{n}| = 1, \qquad \operatorname{div}(\boldsymbol{\epsilon}(\boldsymbol{n})\nabla\psi) = 0 \tag{54}$$

Here γ is a viscosity parameter; $\boldsymbol{h}$ denotes the "molecular field" (the terminology used in de Gennes and Prost[17]),

$$\boldsymbol{h} := -\frac{\delta\sigma}{\delta \boldsymbol{n}} = \operatorname{div}\left(\frac{\partial\sigma}{\partial\nabla\boldsymbol{n}}\right) - \frac{\partial\sigma}{\partial\boldsymbol{n}} \tag{55}$$

and $P(\boldsymbol{n}) := \mathbf{I} - \boldsymbol{n}\otimes\boldsymbol{n}$ gives the projection transverse to the local director. Equation (54) represents the single-rotational-viscosity director dynamics (or gradient flow) associated with our free energy. The director is always constrained to have unit length. The electric field is taken to adjust instantaneously to any changes in the director field—this is justified by the fact that the relaxation time for the electric field is several orders of magnitude smaller than the relaxation time of the liquid-crystal director field (roughly of the order of femtoseconds versus milliseconds). The system is also subject to initial, boundary, and periodic conditions on the fields $\boldsymbol{n}(x, z, t)$ and $\psi(x, z, t)$.

Equilibrium solutions, as defined by Eq. (4), are precisely time-independent solutions of (54). An equilibrium solution is said to be "locally stable" if all sufficiently small perturbations of it, taken as initial conditions in (54), decay back to the equilibrium configuration as $t \to \infty$. Such small perturbations should evolve initially according to the linearization of the system (54) around the equilibrium field, and so we say an equilibrium solution is "linearly stable" if the solutions of the linearized constrained dynamical system (below) decay to zero in time for any initial data.

Thus let us consider an equilibrium state $(\boldsymbol{n}_0, \psi_0)$ and small perturbations of it: $\boldsymbol{n} = \boldsymbol{n}_0 + \boldsymbol{u}$, $\psi = \psi_0 + \chi$, $|\boldsymbol{u}(x, z, t)|, |\chi(x, z, t)| \ll 1$. We substitute these into Eq. (54) and expand to first order in $\boldsymbol{u}$ and χ. The pointwise constraint $|\boldsymbol{n}| = 1$ leads to the condition $\boldsymbol{n}_0 \cdot \boldsymbol{u} = 0$; while the electrostatic equation leads to

$$\operatorname{div}(\boldsymbol{\epsilon}_0\nabla\chi) + \operatorname{div}(\boldsymbol{\epsilon}_0'\nabla\psi_0) = 0 \tag{56}$$

where $\boldsymbol{\epsilon}_0$ and $\boldsymbol{\epsilon}_0'$ are the dielectric tensor and its linearization at the equilibrium solution $\boldsymbol{n}_0$

$$\begin{aligned} \boldsymbol{\epsilon}_0 &= \boldsymbol{\epsilon}(\boldsymbol{n}_0) = \varepsilon_0(\varepsilon_\perp \mathbf{I} + \varepsilon_a \boldsymbol{n}_0 \otimes \boldsymbol{n}_0) \\ \boldsymbol{\epsilon}_0' &= \varepsilon_0\varepsilon_a(\boldsymbol{n}_0 \otimes \boldsymbol{u} + \boldsymbol{u} \otimes \boldsymbol{n}_0) \end{aligned} \tag{57}$$

The dynamical equation for $\boldsymbol{n}$, upon linearization, produces

$$\gamma\frac{\partial \boldsymbol{u}}{\partial t} = P(\boldsymbol{n}_0)\boldsymbol{h}_0 + P(\boldsymbol{n}_0)\boldsymbol{h}_0' - (\boldsymbol{h}_0\cdot\boldsymbol{u})\boldsymbol{n}_0 - (\boldsymbol{h}_0\cdot\boldsymbol{n}_0)\boldsymbol{u} \tag{58}$$

where $\boldsymbol{h}_0$ and $\boldsymbol{h}_0'$ denote the molecular field and its linearization at the equilibrium solution $(\boldsymbol{n}_0, \psi_0)$. This equation can be simplified using the equilibrium conditions:

$$P(\boldsymbol{n}_0)\boldsymbol{h}_0 = \mathbf{0} \;\Rightarrow\; \boldsymbol{h}_0 = \lambda_0\boldsymbol{n}_0, \quad \lambda_0 := \boldsymbol{h}_0\cdot\boldsymbol{n}_0 \tag{59}$$

and

$$\boldsymbol{h}_0\cdot\boldsymbol{u} = \lambda_0\boldsymbol{n}_0\cdot\boldsymbol{u} = 0 \tag{60}$$

Here λ_0 is the Lagrange-multiplier field associated with the pointwise unit-vector constraint on the equilibrium director field $\boldsymbol{n}_0$. This leaves us with the following general form of the linearized constrained dynamical system:

$$\begin{aligned} \gamma\frac{\partial\boldsymbol{u}}{\partial t} &= P(\boldsymbol{n}_0)\boldsymbol{h}_0' - \lambda_0\boldsymbol{u}, \quad \boldsymbol{n}_0\cdot\boldsymbol{u} = 0 \\ \operatorname{div}(\boldsymbol{\epsilon}_0\nabla\chi) &+ \operatorname{div}(\boldsymbol{\epsilon}_0'\nabla\psi_0) = 0 \end{aligned} \tag{61}$$

We note that $\boldsymbol{h}_0'$ is linear in both $\boldsymbol{u}$ and χ, while $\boldsymbol{\epsilon}_0'$ is linear in $\boldsymbol{u}$. Below we write out the explicit form they take for our problem when linearized around the Homeotropic configuration.

5.2. Linear Stability Equations for Homeotropic Configuration

For our case of interest, namely the Homeotropic configuration, the director field is uniformly aligned in the z direction, and the electrostatic potential is a linear profile in z across the cell gap:

$$\boldsymbol{n}_0(z) = \boldsymbol{e}_z, \quad \psi_0(z) = \frac{Vz}{d} \tag{62}$$

The associated Lagrange multiplier field is uniform as well, as is the projection P:

$$\lambda_0(z) = \boldsymbol{h}_0 \cdot \boldsymbol{n}_0 = h_z(\boldsymbol{n}_0, \psi_0) = \varepsilon_0 \varepsilon_a \frac{V^2}{d^2}$$
$$P(\boldsymbol{n}_0) = \boldsymbol{e}_x \otimes \boldsymbol{e}_x + \boldsymbol{e}_y \otimes \boldsymbol{e}_y \tag{63}$$

The expressions for the components of the molecular field, from which the formula for λ_0 above is derived, are given in the Appendix. The pointwise constraint gives

$$\boldsymbol{n}_0 \cdot \boldsymbol{u} = 0 \;\Rightarrow\; \boldsymbol{u} = u\boldsymbol{e}_x + v\boldsymbol{e}_y \tag{64}$$

The dielectric tensor and its linearization are thus given (in Cartesian component form) by

$$\boldsymbol{\epsilon}_0 = \varepsilon_0 \begin{bmatrix} \varepsilon_\perp & & \\ & \varepsilon_\perp & \\ & & \varepsilon_\parallel \end{bmatrix}, \quad \boldsymbol{\epsilon}_0' = \varepsilon_0 \varepsilon_a \begin{bmatrix} 0 & 0 & u \\ 0 & 0 & v \\ u & v & 0 \end{bmatrix} \tag{65}$$

The dynamical equations for u and v take the form

$$\gamma \frac{\partial u}{\partial t} = (\boldsymbol{h}_0')_x - \lambda_0 u \tag{66a}$$
$$\gamma \frac{\partial v}{\partial t} = (\boldsymbol{h}_0')_y - \lambda_0 v \tag{66b}$$

from which we finally arrive at the linearized dynamical system coupling the perturbations u, v, and χ:

$$\gamma u_t = K_1 u_{xx} + K_3 u_{zz} - \varepsilon_0 \varepsilon_a \frac{V^2}{d^2} u + 2K_2 q_0 v_z + \varepsilon_0 \varepsilon_a \frac{V}{d} \chi_x \tag{67a}$$
$$\gamma v_t = K_2 v_{xx} + K_3 v_{zz} - \varepsilon_0 \varepsilon_a \frac{V^2}{d^2} v - 2K_2 q_0 u_z \tag{67b}$$
$$\varepsilon_\perp \chi_{xx} + \varepsilon_\parallel \chi_{zz} + \varepsilon_a \frac{V}{d} u_x = 0 \qquad -\infty < x < \infty,\ 0 < z < d,\ 0 < t \tag{67c}$$

Here $u = u(x, z, t)$, $u_t = \partial u / \partial t$, etc., and this system must be solved subject to homogeneous boundary conditions

$$u = v = \chi = 0, \quad \text{on } z = 0 \text{ or } d \tag{68}$$

and prescribed initial conditions

$$u(x, z, 0) = u_0(x, z), \quad v(x, z, 0) = v_0(x, z)$$
$$\chi(x, z, 0) = \chi_0(x, z) \tag{69}$$

This is a coupled dissipative dynamical system for u and v, with the χ variable slaved to the u variable, producing an effective nonlocal contribution to the right-hand-side of the first equation. Our task is to determine under what conditions on the parameters the solutions to these equations decay in time (linearly stable case) versus grow in time (linearly unstable case).

It is once again useful to nondimensionalize our problem. We do so in a way that is consistent with the scalings we have used previously in (25):

$$\bar{x} := \frac{\pi x}{d}, \quad \bar{z} := \frac{\pi z}{d}, \quad \bar{t} := \frac{t}{\tau}, \quad \tau := \frac{\gamma d^2}{K_3 \pi^2} \tag{70a}$$
$$\bar{u}(\bar{x}, \bar{z}, \bar{t}) := u(x, z, t), \quad \bar{v}(\bar{x}, \bar{z}, \bar{t}) := v(x, z, t)$$
$$\bar{\chi}(\bar{x}, \bar{z}, \bar{t}) := \pi \chi(x, z, t)/V \tag{70b}$$
$$\bar{K}_1 := \frac{K_1}{K_3} = k_1 + 1, \quad \bar{K}_2 := \frac{K_2}{K_3} = k_2 + 1, \quad \bar{\varepsilon}_\perp := \frac{\varepsilon_\perp}{\varepsilon_\parallel} = 1 - \bar{\varepsilon}_a \tag{70c}$$
$$\alpha := \sqrt{\frac{-\varepsilon_0 \varepsilon_a}{K_3}} \frac{V}{\pi}, \quad \beta := \frac{K_2 q_0 d}{K_3 \pi} \tag{70d}$$

Note that $\bar{K}_1$, $\bar{K}_2$, and $\bar{\varepsilon}_\perp$ are all *positive*. The linearized stability system reads (after dropping bars)

$$u_t = \bar{K}_1 u_{xx} + u_{zz} + \alpha^2 u + 2\beta v_z - \alpha^2 \chi_x \tag{71a}$$
$$v_t = \bar{K}_2 v_{xx} + v_{zz} + \alpha^2 v - 2\beta u_z \tag{71b}$$
$$\bar{\varepsilon}_\perp \chi_{xx} + \chi_{zz} + \bar{\varepsilon}_a u_x = 0, \quad -\infty < x < \infty, 0 < z < \pi \tag{71c}$$

The analysis of the previous section corresponds here to the case in which u, v, and χ are *independent of* x, which reduces the above to

$$u_t = u_{zz} + \alpha^2 u + 2\beta v_z \tag{72a}$$
$$v_t = v_{zz} + \alpha^2 v - 2\beta u_z \tag{72b}$$
$$\chi_{zz} = 0 \tag{72c}$$

It follows that in this case $\chi(z, t) = 0$, and as we shall see below, the coupled $u - v$ problem will be asymptotically stable whenever $\alpha^2 + \beta^2 < 1$, which is the same conclusion as reached by the previous (differently executed) 1-D stability analysis.

We are interested in solutions to our general problem that are either uniform in x or periodic in x with some finite period. Thus we consider perturbations of the form

$$u(x, z, t) = e^{iqx} \hat{u}(z, t), \quad v(x, z, t) = e^{iqx} \hat{v}(z, t)$$
$$\chi(x, z, t) = e^{iqx} \hat{\chi}(z, t) \tag{73}$$

where q is an arbitrary real number. Substituting into Eqs. (71), we obtain

$$\hat{u}_t = \hat{u}_{zz} + (\alpha^2 - \bar{K}_1 q^2)\hat{u} + 2\beta \hat{v}_z - iq\alpha^2 \hat{\chi} \tag{74a}$$
$$\hat{v}_t = \hat{v}_{zz} + (\alpha^2 - \bar{K}_2 q^2)\hat{v} - 2\beta \hat{u}_z \tag{74b}$$
$$\hat{\chi}_{zz} - \bar{\varepsilon}_\perp q^2 \hat{\chi} + iq\bar{\varepsilon}_a \hat{u} = 0 \tag{74c}$$

We note that except for the $\hat{\chi}$ coupling between the first and third equations (the effect of which is not yet clear),

RESEARCH ARTICLE

the terms $-\bar{K}_1 q^2$ and $-\bar{K}_2 q^2$ are *stabilizing*: they just have the effect of reducing the effective voltage—recall that $\alpha^2 \propto V^2$.

Equation (74c) plus the boundary conditions $\hat{\chi}(0,t) = \hat{\chi}(\pi,t) = 0$ can be solved explicitly using a Green's function representation:

$$\hat{\chi}(z,t) = iq\bar{\varepsilon}_a \int_0^\pi g(z,\zeta;q)\hat{u}(\zeta,t)\,d\zeta \tag{75}$$

where g is given in terms of its eigenfunction expansion by

$$g(z,\zeta;q) = \frac{2}{\pi}\sum_{k=1}^{\infty}\frac{\sin kz \sin k\zeta}{\mu_k}, \quad \mu_k := k^2 + \bar{\varepsilon}_\perp q^2 \tag{76}$$

It follows that the associated integral operator is *positive definite*, in the sense that

$$\int_0^\pi \int_0^\pi g(z,\zeta;q) f(z) f(\zeta)\,dz\,d\zeta \geq 0 \tag{77}$$

for any square-integrable function f (with equality if and only if f is the zero function). The deflated coupled system that results is

$$\hat{u}_t = \hat{u}_{zz} + (\alpha^2 - \bar{K}_1 q^2)\hat{u} + 2\beta\hat{v}_z + \bar{\varepsilon}_a q^2 \alpha^2 \int_0^\pi g(z,\zeta;q)\hat{u}(\zeta,t)\,d\zeta \tag{78a}$$

$$\hat{v}_t = \hat{v}_{zz} + (\alpha^2 - \bar{K}_2 q^2)\hat{v} - 2\beta\hat{u}_z \tag{78b}$$

The positive definiteness of the integral operator (and the fact that $\bar{\varepsilon}_a$ is a *negative* number) shows us now that the influence of this (nonlocal) term is *stabilizing* as well. We just need to provide an argument for this observation, which we do now.

5.3. Energy Method Analysis

We can use an "Energy Method" type of argument to show that under appropriate conditions on the parameters, the solutions to Eq. (78) decay in time. Define the "energy"

$$E(t) := \frac{1}{2}\int_0^\pi [\hat{u}(z,t)^2 + \hat{v}(z,t)^2]\,dz \tag{79}$$

and note that $E(t) = 0 \Rightarrow \hat{u}(\cdot,t) = \hat{v}(\cdot,t) = 0$. Then using Eq. (78), it follows that

$$\begin{aligned} E'(t) &= \int_0^\pi (\hat{u}\hat{u}_t + \hat{v}\hat{v}_t)\,dz \\ &= \int_0^\pi [-\hat{u}_z^2 + 2\beta(\hat{u}\hat{v}_z - \hat{v}\hat{u}_z) - \hat{v}_z^2]\,dz \\ &\quad + (\alpha^2 - \bar{K}_1 q^2)\int_0^\pi \hat{u}^2\,dz + (\alpha^2 - \bar{K}_2 q^2)\int_0^\pi \hat{v}^2\,dz \\ &\quad + \bar{\varepsilon}_a q^2 \alpha^2 \int_0^\pi \int_0^\pi g(z,\zeta;q)\hat{u}(z,t)\hat{u}(\zeta,t)\,dz\,d\zeta \end{aligned} \tag{80}$$

We claim that the first integral in the expression for $E'(t)$ above satisfies the bound

$$\begin{aligned} J[\hat{u},\hat{v}] &:= \int_0^\pi [-\hat{u}_z^2 + 2\beta(\hat{u}\hat{v}_z - \hat{v}\hat{u}_z) - \hat{v}_z^2]\,dz \\ &\leq (\beta^2 - 1)\int_0^\pi (\hat{u}^2 + \hat{v}^2)\,dz \end{aligned} \tag{81}$$

This follows from the fact that the extremals of J subject to the constraint $\int_0^\pi (\hat{u}^2 + \hat{v}^2)\,dz = 1$ must satisfy the coupled eigenvalue problem

$$\hat{u}_{zz} + 2\beta\hat{v}_z = \lambda\hat{u} \tag{82a}$$

$$\hat{v}_{zz} - 2\beta\hat{u}_z = \lambda\hat{v} \tag{82b}$$

on $0 < z < \pi$ subject to boundary conditions $\hat{u} = \hat{v} = 0$, at $z = 0, \pi$. A complete set of eigenfunctions and associated eigenvalues for this problem is given by

$$\begin{bmatrix}\hat{u}\\ \hat{v}\end{bmatrix}_n = \sin nz \begin{bmatrix}\cos\beta z\\ \sin\beta z\end{bmatrix}, \quad \sin nz \begin{bmatrix}-\sin\beta z\\ \cos\beta z\end{bmatrix}$$
$$\lambda_n = \beta^2 - n^2,\ n = 1, 2, \ldots \tag{83}$$

and $\lambda_{\max} = \lambda_1 = \beta^2 - 1$, which proves (81).

Given the bound (81), and using (77) plus $\bar{\varepsilon}_a < 0$, we obtain from (80)

$$E' \leq rE, \quad r := \alpha^2 + \beta^2 - 1 - q^2 \min\{\bar{K}_1, \bar{K}_2\} \tag{84}$$

By use of an integrating factor, it follows that

$$E(t) \leq e^{rt}E(0) = \frac{1}{2}e^{rt}\int_0^\pi (\hat{u}_0^2 + \hat{v}_0^2)\,dz \tag{85}$$

When the parameters are such that $r < 0$, we have

$$E(t) \to 0, \quad \text{as } t \to \infty \ \Rightarrow\ \hat{u}(\cdot,t), \hat{v}(\cdot,t) \to 0, \quad \text{as } t \to \infty \tag{86}$$

We have established the following.

CLAIM. *Consider the coupled $\hat{u} - \hat{v}$ nonlocal dissipative dynamical system* (78), *subject to homogeneous boundary conditions*

$$\hat{u}(0,t) = \hat{u}(\pi,t) = \hat{v}(0,t) = \hat{v}(\pi,t) = 0 \tag{87}$$

and sufficiently regular initial conditions

$$\hat{u}(z,0) = \hat{u}_0(z), \quad \hat{v}(z,0) = \hat{v}_0(z) \tag{88}$$

If the parameters satisfy

$$\alpha^2 + \beta^2 < 1 + q^2 \min\{\bar{K}_1, \bar{K}_2\} \tag{89}$$

then the solution decays in time:

$$\hat{u}(\cdot,t), \quad \hat{v}(\cdot,t) \to 0, \quad \textit{as } t \to \infty \tag{90}$$

We conclude that for (α, β) inside the spinodal ellipse (23), the Homeotropic configuration is linearly stable with respect to arbitrary 2-D perturbations. As the spinodal threshold is crossed, stability is lost to a uniform-in-x configuration. This uniform-in-x solution could be a TIC or a periodic configuration, such as CF1, of diverging period ($q \to 0$); this is consistent with the qualitative analysis of Ref. [26]. There is never any local instability (direct transition) to a periodic structure of finite period. It should be emphasized that this all is just local linear stability analysis; we know that there are regions inside the spinodal ellipse where TIC and periodic structures coexist with the Homeotropic configuration and have lower free energy.

6. CONCLUSIONS

Through a combination of analytical, numerical, and qualitative techniques, a fairly complete understanding of the phase and bifurcation behavior of the two competing 1-D equilibrium solutions "Homeotropic" and "Translation Independent Cholesteric" (TIC) has been obtained. Our analysis in this paper should be viewed in the context of Ref. [27], with particular attention to the phase diagrams in Figures 1, 4, and 7 of that paper, constructed there from laboratory experiments. We emphasize that in this paper we have constrained all solutions to be functions of z only. In a more general setting, in which the fields were allowed to be functions of both x and z (as is the case with the CF1 configuration), the solutions we have studied here would continue to be equilibria; however their stability properties (both local and global) could change as a result of the larger class of admissible perturbations. In the last section we have shown, however, that the Homeotropic solution remains locally stable to arbitrary periodic-in-x 2-D perturbations for parameters inside the spinodal ellipse.

We find this system to be fairly rich and complicated even in this first-stage analysis (with our restrictive modeling assumptions), which foreshadows developments to follow. An interesting aspect of the system revealed by our analysis is the tilt-dependent nature of the twist rate of the TIC solution, and as a result the voltage-dependent nature of the total twist across the cell, as given in Eq. (18). While this general phenomenon is familiar in the dynamical setting (because of its relevance to switching dynamics in cholesteric devices), we have here a clean and explicit realization of it in an equilibrium setting.

The analysis of the Homeotropic-TIC transition held some surprises. Upon identification of the transition point on the spinodal ellipse where the Homeotropic-TIC bifurcation changed from supercritical to subcritical, one certainly anticipated that this would simply be a tricritical point where the phase transition changed from 2nd order to 1st order. Instead one finds a range of parameters where two different types of TIC solutions (small vs. large amplitude) coexist; one finds as well accompanying "S-shaped" bifurcating solution branches. In the end, this may not be highly relevant, as the CF1 solution appears to have lower free energy in that region, and so it is possible that these other metastable configurations may not be observable via laboratory experiments. The linear stability analysis of the Homeotropic configuration with respect to arbitrary 2-D perturbations rules out the possibility of any direct transitions from Homeotropic to any periodic-in-x solutions.

While this is just a first phase of our analysis of this system, the implications of it (and also of the experimental work in Ref. [27]) for potential technological applications may be important. An "ideal" system would be one that just admitted two, robust, stable configurations of the Homeotropic and TIC type, with the TIC "opening up," as voltage is increased, to a continuously larger maximum tilt angle while maintaining a constant total twist across the cell gap. The actual system differs from this in some ways. First, the total twist is a function of the maximum tilt angle (controlled by voltage) and changes roughly by a factor of *two* as the maximum tilt angle varies from close to zero to close to $\pi/2$. Next, for certain values of the parameters, there are actually two different types of TIC solutions (one with a smaller maximum tilt angle than the other), and there is a 1st-order transition from one to the other as the ratio of cell gap to intrinsic cholesteric pitch d/P or the voltage V (or both) is increased. Finally, for the proprietary material used in the experiments in Ref. [27], we obtain an effective upper bound of roughly $d/P \lesssim 0.9$ for the system to support a simple voltage-driven second-order transition between the Homeotropic and TIC configurations, which limits parameter ranges for technologies based on these states and this transition. In reality, the limit is in fact lower, due to instabilities to periodic-in-x distortions that arise in the range $0.6 \lesssim d/P \lesssim 0.75$, as illustrated in Ref. [27].

APPENDIX: FORMULAS FOR MOLECULAR FIELD IN COMPONENT FORM

In order to simplify some formulas, both for numerical implementation and for analysis, we make use of the relations

$$|\operatorname{curl} \boldsymbol{n}|^2 = (\boldsymbol{n} \cdot \operatorname{curl} \boldsymbol{n})^2 + |\boldsymbol{n} \times \operatorname{curl} \boldsymbol{n}|^2$$
$$\boldsymbol{n} \times \operatorname{curl} \boldsymbol{n} = -(\nabla \boldsymbol{n})\boldsymbol{n} \quad \text{(A1)}$$

valid for smooth vector fields satisfying $|\boldsymbol{n}(\boldsymbol{r})| = 1$, to express the free-energy density from Eq. (2) in the somewhat simpler form

$$\begin{aligned} 2\sigma = {} & K_1(\operatorname{div} \boldsymbol{n})^2 + K_2|\operatorname{curl} \boldsymbol{n}|^2 + 2K_2 q_0(\boldsymbol{n} \cdot \operatorname{curl} \boldsymbol{n}) \\ & + K_2 q_0^2 + (K_3 - K_2)|(\nabla \boldsymbol{n})\boldsymbol{n}|^2 \\ & - \varepsilon_0[\varepsilon_\perp |\nabla \psi|^2 + \varepsilon_a (\nabla \psi \cdot \boldsymbol{n})^2] \end{aligned} \quad \text{(A2)}$$

RESEARCH ARTICLE

For our problem, $\boldsymbol{n} = \boldsymbol{n}(x, z)$ and $\psi = \psi(x, z)$, and we have

$$\operatorname{div} \boldsymbol{n} = n_{x,x} + n_{z,z}, \quad \operatorname{curl} \boldsymbol{n} = \begin{bmatrix} -n_{y,z} \\ n_{x,z} - n_{z,x} \\ n_{y,x} \end{bmatrix}$$
$$(\nabla \boldsymbol{n})\boldsymbol{n} = \begin{bmatrix} n_x n_{x,x} + n_z n_{x,z} \\ n_x n_{y,x} + n_z n_{y,z} \\ n_x n_{z,x} + n_z n_{z,z} \end{bmatrix} \tag{A3}$$

Using these formulas, we can write the free energy (2) in component form

$$\begin{aligned} 2\sigma = {} & K_1(n_{x,x} + n_{z,z})^2 + K_2[n_{y,z}^2 + (n_{x,z} - n_{z,x})^2 + n_{y,x}^2] \\ & + 2K_2 q_0[-n_x n_{y,z} + n_y(n_{x,z} - n_{z,x}) + n_z n_{y,x}] + K_2 q_0^2 \\ & + (K_3 - K_2)[(n_x n_{x,x} + n_z n_{x,z})^2 + (n_x n_{y,x} + n_z n_{y,z})^2 \\ & \qquad + (n_x n_{z,x} + n_z n_{z,z})^2] \\ & - \varepsilon_0[\varepsilon_\perp(\psi_x^2 + \psi_z^2) + \varepsilon_a(n_x\psi_x + n_z\psi_z)^2] \end{aligned} \tag{A4}$$

The components of the molecular field are given in general in the form

$$h_x = \frac{\partial}{\partial x}\left(\frac{\partial \sigma}{\partial n_{x,x}}\right) + \frac{\partial}{\partial z}\left(\frac{\partial \sigma}{\partial n_{x,z}}\right) - \frac{\partial \sigma}{\partial n_x} \tag{A5a}$$

$$h_y = \frac{\partial}{\partial x}\left(\frac{\partial \sigma}{\partial n_{y,x}}\right) + \frac{\partial}{\partial z}\left(\frac{\partial \sigma}{\partial n_{y,z}}\right) - \frac{\partial \sigma}{\partial n_y} \tag{A5b}$$

$$h_z = \frac{\partial}{\partial x}\left(\frac{\partial \sigma}{\partial n_{z,x}}\right) + \frac{\partial}{\partial z}\left(\frac{\partial \sigma}{\partial n_{z,z}}\right) - \frac{\partial \sigma}{\partial n_z} \tag{A5c}$$

For our free energy above, these take the form

$$\begin{aligned} h_x = {} & \frac{\partial}{\partial x}[K_1(n_{x,x} + n_{z,z}) + (K_3 - K_2)(n_x n_{x,x} + n_z n_{x,z})n_x] \\ & + \frac{\partial}{\partial z}[K_2(n_{x,z} - n_{z,x}) + (K_3 - K_2)(n_x n_{x,x} + n_z n_{x,z})n_z] \\ & - (K_3 - K_2)[(n_x n_{x,x} + n_z n_{x,z})n_{x,x} \\ & \qquad + (n_x n_{y,x} + n_z n_{y,z})n_{y,x} + (n_x n_{z,x} + n_z n_{z,z})n_{z,x}] \\ & + 2K_2 q_0 n_{y,z} + \varepsilon_0 \varepsilon_a (n_x\psi_x + n_z\psi_z)\psi_x \end{aligned} \tag{A6a}$$

$$\begin{aligned} h_y = {} & \frac{\partial}{\partial x}[K_2 n_{y,x} + (K_3 - K_2)(n_x n_{y,x} + n_z n_{y,z})n_x] \\ & + \frac{\partial}{\partial z}[K_2 n_{y,z} + (K_3 - K_2)(n_x n_{y,x} + n_z n_{y,z})n_z] \\ & + 2K_2 q_0 (n_{z,x} - n_{x,z}) \end{aligned} \tag{A6b}$$

$$\begin{aligned} h_z = {} & \frac{\partial}{\partial x}[K_2(n_{z,x} - n_{x,z}) + (K_3 - K_2)(n_x n_{z,x} + n_z n_{z,z})n_x] \\ & + \frac{\partial}{\partial z}[K_1(n_{x,x} + n_{z,z}) + (K_3 - K_2)(n_x n_{z,x} + n_z n_{z,z})n_z] \\ & - (K_3 - K_2)[(n_x n_{x,x} + n_z n_{x,z})n_{x,z} \\ & \qquad + (n_x n_{y,x} + n_z n_{y,z})n_{y,z} + (n_x n_{z,x} + n_z n_{z,z})n_{z,z}] \\ & - 2K_2 q_0 n_{y,x} + \varepsilon_0 \varepsilon_a (n_x\psi_x + n_z\psi_z)\psi_z \end{aligned} \tag{A6c}$$

Acknowledgments: This work is part of the AlphaMicron/TAF collaborative project "Liquid Crystal Eyewear," supported in part by the State of Ohio and AlphaMicron, Inc. E. C. Gartland Jr. also acknowledges support of the National Science Foundation, Grant Nos. DMS-0456221 and DMS-0608670. O. D. Lavrentovich and I. I. Smalyukh acknowledge the support of NSF, Grant Nos. DMR-0315523 and DMR-0504516. I. I. Smalyukh also acknowledges the support of the International Institute for Complex Adaptive Matter and NSF, Grant No. DMR-0645461.

References

1. L. M. Blinov and V. G. Chigrinov, Electrooptic Effects in Liquid Crystal Materials, Springer-Verlag, New York (**1994**).
2. P. F. McManamon, T. A. Dorschner, D. L. Corkum, L. J. Friedman, D. S. Hobbs, M. Holz, S. Liberman, H. Q. Nguyen, D. P. Resler, R. C. Sharp, and E. A. Watson, *Proc. IEEE* 84, 268 (**1996**).
3. J. S. Patel and G. B. Cohen, *Appl. Phys. Lett.* 68, 3564 (**1996**).
4. D.-K. Yang, X.-Y. Huang, and Y.-M. Zhu, *Annu. Rev. Mater. Sci.* 27, 117 (**1997**).
5. P. Palffy-Muhoray, *Nature* 391, 745 (**1998**).
6. B. Taheri, P. Palffy-Muhoray, T. Kosa, and D. L. Post, *Proc. SPIE* 4021, 114 (**2000**).
7. O. D. Lavrentovich and M. Kleman, Chirality in Liquid Crystals, edited by C. Bahr and H.-S. Kitzerow, Springer-Verlag, New York (**2001**), Chapter 5, pp. 115–158.
8. F. A. Muñoz, P. Palffy-Muhoray, and B. Taheri, *Opt. Lett.* 26, 804 (**2001**).
9. J. Schmidtke, W. Stille, and H. Finkelmann, *Phys. Rev. Lett.* 90, 083902 (**2003**).
10. J.-S. Hsu, B.-J. Liang, and S.-H. Chen, *Appl. Phys. Lett.* 85, 5511 (**2004**).
11. M. F. Moreira, I. C. S. Carvalho, W. Cao, C. Bailey, B. Taheri, and P. Palffy-Muhoray, *Appl. Phys. Lett.* 85, 2691 (**2004**).
12. B. I. Senyuk, I. I. Smalyukh, and O. D. Lavrentovich, *Opt. Lett.* 30, 349 (**2005**).
13. E. B. Priestley, P. J. Wojtowicz, and P. Sheng, eds., Introduction to Liquid Crystals, Plenum Press, New York and London (**1975**).
14. G. Vertogen and W. H. de Jeu, Thermotropic Liquid Crystals, Fundamentals, Springer-Verlag, Berlin Heidelberg (**1988**).
15. S. A. Pikin, Structural Transformation in Liquid Crystals, Gordon and Breach Science Publishers, New York (**1991**).
16. S. Chandrasekhar, Liquid Crystals, 2nd edn., Cambridge University Press, Cambridge (**1992**).
17. P. G. de Gennes and J. Prost, The Physics of Liquid Crystals, 2nd edn., Clarendon Press, Oxford (**1993**).
18. M. Kleman and O. D. Lavrentovich, Soft Matter Physics: An Introduction, Springer-Verlag, New York (**2003**).
19. J. L. Ericksen and D. Kinderlehrer, eds., Theory and Applications of Liquid Crystals, Springer-Verlag, New York (**1987**).
20. E. G. Virga, Variational Theories for Liquid Crystals, Chapman & Hall, London (**1994**).
21. I. W. Stewart, The Static and Dynamic Continuum Theory of Liquid Crystals: A Mathematical Introduction, Taylor & Francis, London (**2004**).
22. M. J. Press and A. S. Arrott, *J. Phys. (France)* 37, 387 (**1976**).
23. M. J. Press and A. S. Arrott, *Mol. Cryst. Liq. Cryst.* 37, 81 (**1976**).
24. P. Ribiére, S. Pirkl, and P. Oswald, *Phys. Rev. A* 44, 8198 (**1991**).
25. J. Baudry, S. Pirkl, and P. Oswald, *Phys. Rev. E* 57, 3038 (**1998**); 59, 5562 (**1999**).
26. P. Oswald, J. Baudry, and S. Pirkl, *Physics Reports* 337, 67 (**2000**).

27. I. I. Smalyukh, B. I. Senyuk, V. Bodnar, T. Kosa, B. Taheri, H. Huang, E. C. Gartland, Jr., P. Palffy-Muhoray, and O. D. Lavrentovich, *Phys. Rev. E* 72, 061707 **(2005)**.
28. I. F. Lyuksyutov, *Zh. Eksp. Teor. Fiz.* 75, 358 **(1978)**; *Sov. Phys. JETP* 48, 178 **(1978)**.
29. A. A. Sonin, The Surface Physics of Liquid Crystals, Gordon and Breach, Amsterdam **(1995)**.
30. H. Yokoyama, Handbook of Liquid Crystal Research, edited by P. J. Collings and J. S. Patel, Oxford University Press, New York **(1997)**, Chapter 6, pp. 179–235.
31. H. J. Deuling, *Mol. Cryst. Liq. Cryst.* 19, 123 **(1972)**.
32. A. Dhooge, W. Govaerts, and Yu. A. Kuznetsov, *ACM Trans. Math. Software* 29, 141 **(2003)**.
33. F. Lonberg and R. B. Meyer, *Phys. Rev. Lett.* 55, 718 **(1985)**.

Received: 6 January 2008. Accepted: 3 July 2008.